

Antarctic grounding line mapping from differential satellite radar interferometry

E. Rignot,^{1,2} J. Mouginot,¹ and B. Scheuchl¹

Received 15 February 2011; revised 2 April 2011; accepted 6 April 2011; published 26 May 2011.

[1] The delineation of an ice sheet grounding line, i.e., the transition boundary where ice detaches from the bed and becomes afloat in the ocean, is critical to ice sheet mass budget calculations, numerical modeling of ice sheet dynamics, ice-ocean interactions, oceanic tides, and subglacial environments. Here, we present 15 years of comprehensive, high-resolution mapping of grounding lines in Antarctica using differential satellite synthetic-aperture radar interferometry (DInSAR) data from the Earth Remote Sensing Satellites 1–2 (ERS-1/2), RADARSAT-1 and 2, and the Advanced Land Observing System (ALOS) PALSAR for years 1994 to 2009. DInSAR directly measures the vertical motion of floating ice shelves in response to tidal oceanic forcing with millimeter precision, at a sample spacing better than 50 m, simultaneously over areas several 100 km wide; in contrast with earlier methods that detect abrupt changes in surface slope in satellite visible imagery or altimetry data. On stagnant and slow-moving areas, we find that breaks in surface slope are reliable indicators of grounding lines; but on most fast-moving glaciers and ice streams, our DInSAR results reveal that prior mappings have positioning errors ranging from a few km to over 100 km. A better agreement is found with ICESat's data, also based on measurements of vertical motion, but with a detection noise one order of magnitude larger than with DInSAR. Overall, the DInSAR mapping of Antarctic grounding lines completely redefines the coastline of Antarctica.

Citation: Rignot, E., J. Mouginot, and B. Scheuchl (2011), Antarctic grounding line mapping from differential satellite radar interferometry, *Geophys. Res. Lett.*, 38, L10504, doi:10.1029/2011GL047109.

1. Introduction

[2] The grounding line, G, is the transition boundary between ice in contact with the bed and ice afloat in the ocean waters. This line migrates back and forth with changes in oceanic tides over a “grounding zone” that varies in width depending on the slopes of the glacier bed and surface, and the amplitude of tides. The grounding line position is difficult to identify in situ [e.g., Horgan and Anandakrishnan, 2006]. It has been mapped extensively using visible satellite imagery [Swithinbank, 1988; Bohlander and Scambos, 2007] and more recently using differential satellite radar interferometry (DInSAR) [Rignot, 1996, 1998a, 1998b, 2001, 2002;

Gray et al., 2002; Joughin and Bamber, 2005; Rignot et al., 2008] and ICESat [Brunt et al., 2010].

[3] Knowing the position of the grounding line is critical for mass budget calculations because it determines the precise location of where ice detaches from the bed and becomes afloat in the ocean, typically far upstream (10 to 1,000 km) from where ice calves into icebergs. It is near the grounding line that ice shelves experience the largest rates of melting by the ocean [Rignot and Jacobs, 2002]. Ice fluxes calculated seaward of grounding lines are significantly lower (up to 100%) and may erroneously suggest that glaciers are not discharging enough ice to maintain mass equilibrium, or that ice shelves are not melting as much from the bottom (up to 100%) [e.g., Rignot, 1998a]. The grounding zone is also where ice reaches hydrostatic equilibrium for the first time, so ice thickness may be calculated from ice-surface elevation where no radio echo soundings exist.

[4] The grounding line is a fundamental transition for ice dynamics. It is the locus of a major shift in ice flow from shear-dominated, basal-drag-controlled ice stream flow to drag-free, side-shear-controlled, gravity spreading of floating ice shelves onto the ocean. Modeling of this transition zone is a major challenge in modern numerical modeling of ice sheet flow [Gillet-Chauvet and Durand, 2010; Vieli and Payne, 2005]. Grounding line dynamics govern the retreat and advance of glaciers because they modulate the buttressing resistance to flow [e.g., Thomas et al., 2004]. To make progress in our understanding of grounding-line dynamics, it is essential to have a precise and reliable knowledge of grounding line positions. In addition, surface velocities are conveniently equal to depth-averaged velocities at G because ice shelves experience no vertical shear. And finally, the grounding line position is a sensitive indicator of glacier change. With glacier slopes typically lower than 1% in the transition region, meter-scale changes in ice thickness translate into grounding line migrations of 100 m's, i.e., two orders of magnitude larger, which is detectable with DInSAR [Rignot, 1998a].

[5] Here, we summarize 15 years of DInSAR mapping in Antarctica using a suite of satellites that provide the first complete, high-precision, uniform sampling mapping of all Antarctic grounding lines, including areas south of 81°S covered for the first time in 2009. We compare our results with prior mappings and discuss the impact of our findings on our general knowledge of the Antarctic coastline.

2. Data and Methodology

[6] A schematic of the grounding zone is shown in Figure 1 based on actual data from Petermann Gletscher, Greenland to compare various approaches to grounding line mapping [Smith, 1991; Rignot, 1996]. Actual distances and amplitudes

¹Department of Earth System Science, University of California, Irvine, California, USA.

²Jet Propulsion Laboratory, California Institute of Technology, Pasadena, California, USA.

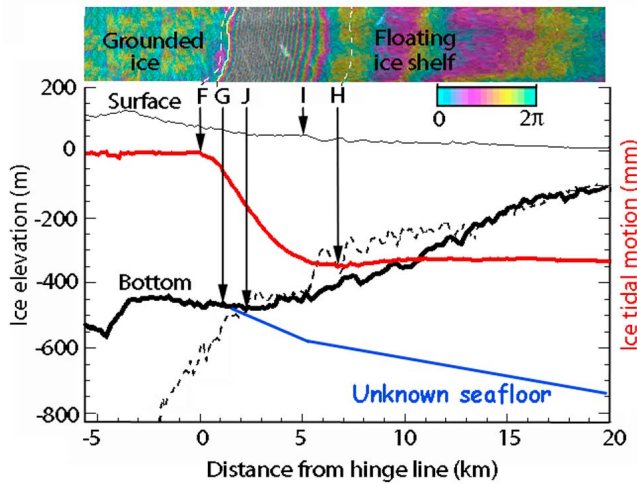


Figure 1. Grounding zone of Petermann Glacier, Greenland, with the limit of tidal flexing (F), the grounding line (G), the line of first hydrostatic equilibrium (J), the break in surface slope (I), the maximum extent of the flexure zone (H), ice surface elevation above mean sea level from laser altimetry (thin black line), bed topography from radio echo sounding (thick black line), bed depth calculated from hydrostatic equilibrium (dashed black line), the unknown seafloor (over-deepening likely exceeds 800 m) and tidal flexing measured with ERS-1 DInSAR in millimeter of vertical motion (red thick line). The color inset on top shows the DInSAR interferometric fringes, color coded from 0 and 2π , from blue to yellow, red and blue, and delineates F (dotted white line near G), G (white line), and H (dotted white on floating ice). Ice flows from left (grounded ice) to right (floating ice).

vary from one glacier to the next. The limit of tidal flexing, F, is the inland extent of tidal flexing. F is not detected with DInSAR but may be calculated by fitting the pattern of vertical motion with an elastic beam model [Rignot, 1998b]. F is 500 m to 1 km upstream of the grounding line, G. G is where ice lifts up from the bed. Point I marks a break in surface slope detectable in satellite visible imagery, photogrammetry or radar altimetry, typically a few km downstream of G. Point H marks the end of the flexure zone if ice deforms elastically. In reality, ice deforms visco-elastically [Schmeltz et al., 2002; Reeh et al., 2003], so tidal flexure exists beyond H. In addition, ice thickness at H is much lower than at G because of ice melting by the ocean in between, so H is not useful for calculating grounding line fluxes. The flexure zone F-H is generally 6–7 km wide in north Greenland, 9–11 km wide on thicker Antarctic glaciers, but larger values (25 km) are observed in areas that are lightly grounded or where tidal flexing is highly contorted by boundary conditions. J is where ice reaches hydrostatic equilibrium for the first time, typically 500 m to 1 km from G. J is difficult to position because it requires a precise knowledge of ice surface elevation, ice thickness, density of seawater and firm depth correction, all of which may vary spatially. Ice is depressed below hydrostatic equilibrium between J and H and is slightly above hydrostatic equilibrium between G and J [e.g., Rignot et al., 1997; Rignot, 2001]. Ice does not reach full, stable hydrostatic equilibrium until beyond H. If we assume hydrostatic equilibrium at G, the error in calculated

ice thickness averages 80 ± 20 m in Antarctica [Rignot et al., 2008]. Here, we map G directly with DInSAR, by positioning it at the inner limit of tidal motion, i.e., where vertical motion of ice is detected for the first time above the noise level (Figure 1).

[7] We use data from the Earth Remote Sensing Satellite 1 and 2 (ERS-1/2) for years 1992, 1994, and 1996 in the Antarctic Peninsula, West Antarctica north of 81°S , Victoria Land and Wilkes Land in East Antarctica; RADARSAT-1 in year 2000 in East Antarctica; RADARSAT-2 in year 2009 for areas south of 81°S ; and ALOS PALSAR in 2007–2008 in select areas north of 77.6°S (Figure 2). The technique is satellite independent. Data from multiple satellites are co-registered with a precision better than 50 m. Multiple mappings are done in some areas to evaluate short term and long term grounding line migrations. The premises of DInSAR are described by Rignot [1996] and will not be repeated here. We difference two interferograms spanning the same time interval (or scaled to be so) with the exact same imaging geometry, i.e., acquired along the same satellite track. A key component of our analysis is to migrate image pixels before forming the interferograms by first calculating the motion field using a speckle tracking technique [Michel and Rignot, 1999] and then displace the image pixels accordingly to restore phase coherence. Each interferogram measures range displacements caused by surface topography (stereoscopic effect), imaging geometry (interferometric baseline), the mostly horizontal and steady creep-flow of ice driven by sliding and gravity (glacier flow), the vertical flapping of the glacier up and down with oceanic tides (tidal motion), plus noise. The differencing removes the glacier flow signal. Surface topography if known is removed, otherwise we select interferograms with a short differential baseline so no topographic correction is required. Tidal motion has a distinct signature of elastic bending that is easily separated from atmospheric/ionospheric errors (random blobs/streaks of artificial motion), surface drawdown (only observed on grounded ice), changes in snow depth (large scale features), or glacier acceleration (tidal motion is smeared). Grounding lines are mapped in the range domain to preserve the original resolution of the data (10 m) and georeferenced to an Earth-fixed grid using Bamber et al.'s [2009] digital elevation model.

[8] Mapping G using a single interferogram is exceptional or rare on ice streams [Goldstein et al., 1993], if not misleading. It is only practical in areas of very low longitudinal stresses, where horizontal strain rates are negligible compared to vertical strain rates associated with tidal flexure. Approaches based on spatial coherence in single interferograms suffer from the same shortcoming [Gray et al., 2002; Joughin and Bamber, 2005]. Phase coherence drops at H as regularly-spaced interferometric fringes (360 degree variation in phase) associated with ice shelf flow on water suddenly mix up with tidal fringes. At G, phase coherence is only restored if grounded ice is nearly stagnant or slow moving, e.g., on an ice rise; otherwise phase coherence decreases again at G as ice motion over a rough bed complicates the pattern of interferometric fringes. As a result, the technique is more likely to detect H than G (see below).

[9] The quality of grounding line mapping depends on the satellite data used (ERS-1/2 and RADARSAT-1/2 are better than ALOS PALSAR), the length of the interferometric baseline (short baselines yield more accurate positioning),

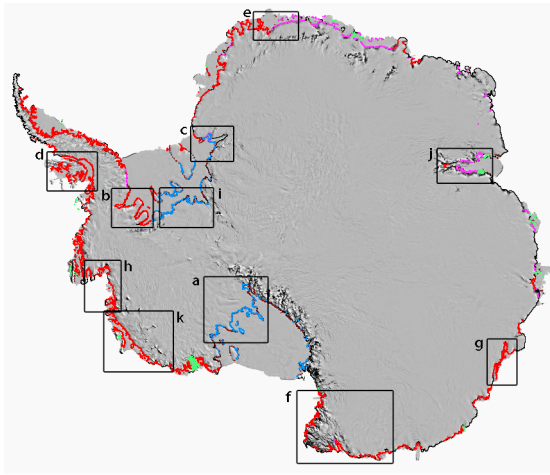


Figure 2. Delineation of Antarctic grounding lines with differential satellite radar interferometry (DInSAR) using ERS-1/2 (red), RADARSAT-1 (purple), RADARSAT-2 (blue), ALOS PALSAR (green) and MOA (brown) overlaid on a MODIS mosaic [Haran et al., 2006]. Rectangles correspond to areas in Figure 3.

the amplitude of the differential tides (larger changes in tide ease the detection of G), and phase coherence (high phase coherence means less noise). If data quality is high, G may be positioned slightly closer to F because the detection noise goes down. To estimate the positional accuracy of G, we compare results from multiple mappings, multiple instruments, and multiple epochs. We find a standard error of ± 100 m. Locally, greater variations are observed, and in some cases, we detect large (km) short-term and long-term migrations [Schmeltz et al., 2001].

3. Results

[10] We mapped 1.4 million grounding line points experiencing tidal flexure (Figure 2). On a 1-km grid, the Antarctic coastline digitized from a 2007–2008 PALSAR radar mosaic is 37,800 km in length. Ice reaches the ocean at over 28,600 km of the coastline, or 76% of Antarctica, of which 22,600 km experiences tidal flexure. Grounding line mapping is complete in the Peninsula and West Antarctica. Gaps exist for glaciers crossing the TransAntarctic mountains and on a few East Antarctic ice shelves (Figure 2). We now compare the DInSAR mapping with the comprehensive mapping from MOA [Bohlander and Scambos, 2007] and the mapping from ICESat [Brunt et al., 2010].

[11] On Siple Coast (Figure 3a), we find an excellent agreement between DInSAR and ICESat. The two techniques use the same detection principle, but with a noise of 10–20 cm or more with ICESat [Brunt et al., 2010] versus 1 cm or smaller with DInSAR [Rignot, 1998b], i.e., 1 to 2 orders of magnitude lower. ICESat coverage is limited to single tracks acquired at different epochs and the track spacing increases northward. DInSAR provides a seamless snapshot of tidal flexing, at all latitudes, simultaneously over swaths that are 75 to 120 km wide. DInSAR confirms the complexity of the grounding zone near Cray Ice Rise, which is not an ice rise but a natural extension of the ice

sheet [Brunt et al., 2010]. On Mercer Ice Stream, G extends 50 km farther south than delineated by MOA, but in agreement with ICESat except for one tributary.

[12] On Evans Ice Stream (Figure 3b), G mapped using 1994 DInSAR data is 50–100 km farther inland than with MOA and there is no ICESat point. The complex spreading of Evans Ice Stream grounding line results from the merging of 4 tributaries of different ice thickness. This situation is not unique to Evans Ice Stream and generates a contorted grounding line where the flexure varies from 6 to 24 km wide. Our DInSAR mapping was critical to an airborne science deployment [Vaughan et al., 2003]. When comparing our mapping with Joughin and Bamber's [2005] based on phase coherence, however, Sykes et al. [2009] report an offset of up to 9 km. This offset is due to the phase coherence method detecting H instead of G. Such a large offset may be common to this method and may explain the large positive mass balance calculated by Joughin and Bamber [2005] who neglected bottom melting near G. On Slessor Glacier (Figure 3c), the ICESat delineation agrees with DInSAR, while MOA's is 100–150 km too far inland. Multiple ice rises are detected with DInSAR, and we observe short-term migrations of 2–3 km of a few grounding line lobes with DInSAR. This indicates a strong sensitivity to tides, i.e., the presence of areas where the ice surface is close to hydrostatic equilibrium or areas of ephemeral grounding [Schmeltz et al., 2001]. Many ice rises are detected also in the mouth of Bailey Ice Stream, where G extends 20 km farther inland than suggested by the few points retrieved from ICESat, hence illustrating the need for dense sampling of grounding lines.

[13] In the Antarctic Peninsula, we find a large concentration of ice rises in the middle of Wilkins Ice Shelf (Figure 3d) that explains its near stagnation and suggests only a thin water column under the ice shelf that must limit ice-ocean interactions. The agreement between DInSAR, MOA and ICESat is equally good along the flanks of George VI Ice Shelf. On Fimbul Ice Shelf (Figure 3e), MOA, ICESat and DInSAR agree, except for Jutulstraumen where MOA's grounding line is 15–20 km too north.

[14] In Victoria Land (Figure 3f), the disparity between DInSAR and MOA exceeds 50 km on many glaciers: seaward on Aviator, Borchgrevink, and Tucker glaciers; and landward on Lille, Rennick and Matusevitch glaciers. This demonstrates that an apparent break in surface slope is not a reliable indicator of G. On Rennick Glacier, ICESat detects grounding in the middle of the ice shelf at 71°S, at a location that coincides with the MOA delineation. DInSAR however reveals that this is only an ice rise; the actual grounding line lays 50 km farther inland, in a much deeper, encroached position, with an ice shelf area 25% larger in size. Farther east, we detect no tidal motion on the eastern half of Cook Ice Shelf, i.e., its ice front is grounded, whereas MOA reports a grounding line 25 km farther inland, which is incompatible with the pattern of tidal motion. This ice shelf reportedly broke off in the 1970s [Frezzotti et al., 1998]. On David Glacier, thick ice flows through a sinuous, deep channel more than 2 km below sea level [Swithinbank, 1988] and tidal bending extends over 25 km, twice longer than for typical Antarctic glaciers.

[15] On Totten Glacier (Figure 3g), G extends along two symmetric lobes of ephemeral grounding stretching 20 km inland and affecting a major fraction of the glacier [Rignot,

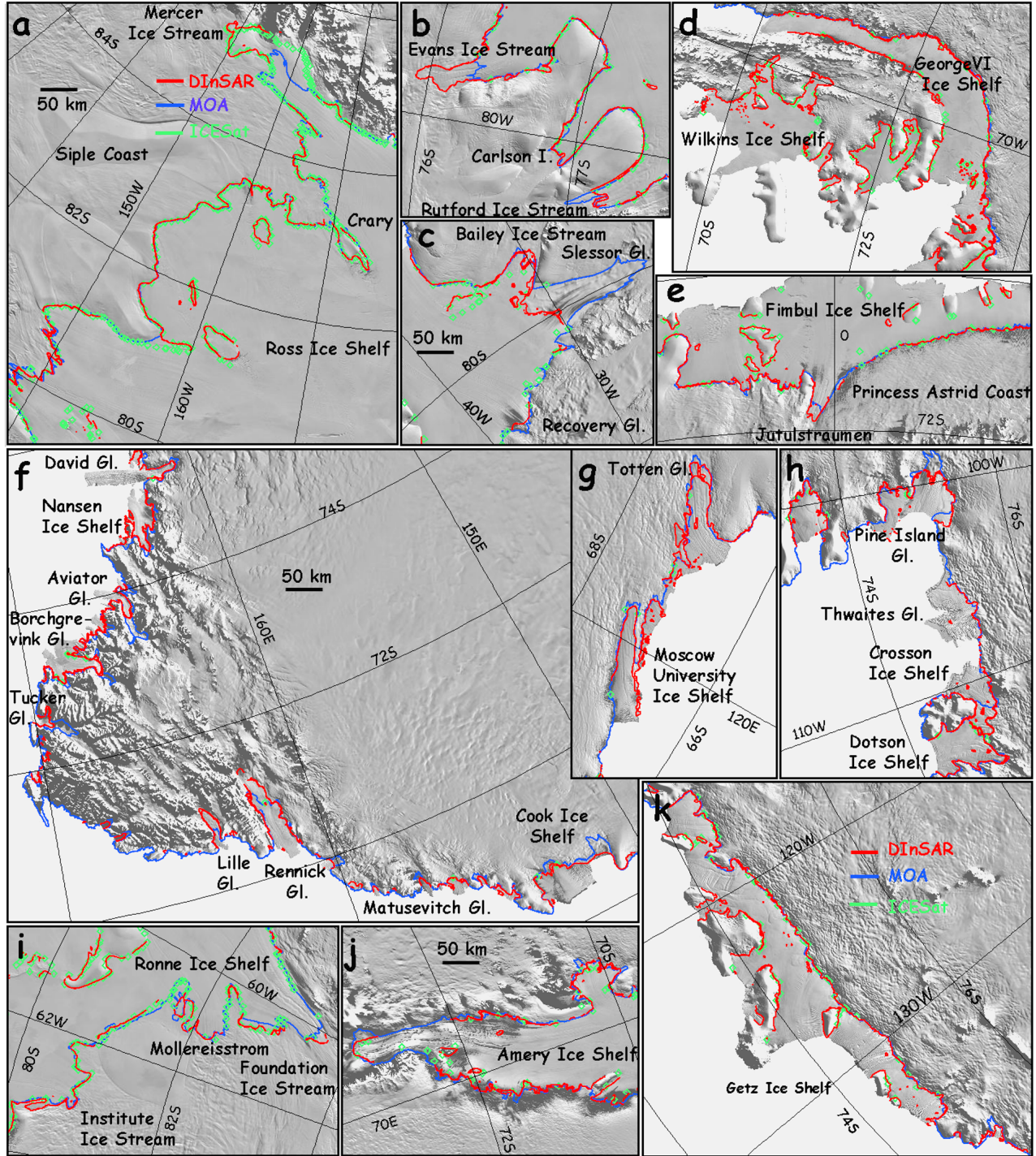


Figure 3. Antarctic grounding lines mapped with DInSAR (red), MOA (dark purple), and ICESat (green diamonds) in areas a–k of Figure 2 with glacier names overlaid on a MODIS mosaic [Haran et al., 2006]. The horizontal scale in Figure 3a applies to all panels.

2002]. Ice along these lobes must be only a few m above hydrostatic equilibrium. We detect numerous ice rises on the ice shelf, including one at its center. On Moscow University Ice Shelf, we also detect numerous ice rises on the northernmost ice shelf, which is separated from the faster-moving southern ice shelf by a grounded ridge several km wide that is parallel to the coast.

[16] On Pine Island Glacier (Figure 2h), MOA places G at the inner edge of an already identified ice plain, 20 km upstream of the 1996 DInSAR position, in a region where no tidal motion is detected. Similarly, MOA's delineation of Crosson and Dotson Ice Shelves is 30 km off and suggests the presence of a grounded ridge between the two ice shelves. The DInSAR mapping instead reveals that the two sub-ice-shelf cavities are linked via a channel inter-spaced

with numerous ice rises but otherwise entirely afloat [Rignot *et al.*, 2004, Figure 4]. On Institute Ice Stream (Figure 3i), DInSAR agrees with ICESat and MOA, but the MOA grounding lines of Mollereisstrom and Foundation Ice Stream are 10 km too far downstream. On Amery Ice Shelf (Figure 3j), G is 120 km inland of where first positioned by Budd *et al.* [1982] near an ice rise. ICESat yields a few points at the southernmost extent of the grounding line that agree with DInSAR, whereas MOA is incorrect on the western flank of the glacier. On Getz Ice Shelf, all three delineations are in agreement. In his area, the break in surface slope at the grounding line is prominent (Figure 3k). Finally, Byrd Glacier (not shown in Figure 3) contrasts with all other glaciers crossing the TransAntarctic mountains, in that G is located mid-way through the terminal valley, 40 km upstream of the Ross Ice Shelf, in ice more than 2.5 km thick.

4. Discussion

[17] While a good agreement exists between DInSAR and MOA in areas of slow flow or steep surface gradients (e.g., Getz Ice Shelf, George VI Ice Shelf, and Princess Astrid Coast), such areas are few. In nearly all areas of fast flow, the MOA delineation is in large disagreement with tidal motion recorded by DInSAR. Grounding lines are mislocated inland or seaward, by several km up to 100–150 km. Improving the resolution of the imagery or the precision of surface slopes would not improve the detectability of G. The fundamental limitation in these areas is that there is no marked break in surface slope at G. The explanation is probably that ice streams are already fully sliding on their bed at G, flowing nearly like ice shelves, so the transition in flow style between shear-stress dominated grounded ice to zero-basal-resistance ice shelves produces a more gradual change in surface slope. In many places, we also note that the presence of ice rises in the middle of ice shelves can be misinterpreted as evidence for grounding of the entire ice shelf system (e.g., Amery, Rennick, Bailey, Slessor glaciers).

[18] The mislocation of G of Amery Ice Shelf is notorious [Fricker *et al.*, 2009] because it led to the suggestion that this region was rapidly gaining mass. When the actual grounding line is used to calculate ice thickness, the glacier mass budget is in balance [Rignot *et al.*, 2008], which is consistent with the absence of observed changes in surface elevation. Here, we show that the same problem may be found in many other places, all across Antarctica, if unreliable grounding lines are used. If G is mis-located by 25 to 50 km, the effective ice shelf area may be 100% in error, e.g., on Aviator Glacier. Such errors yield large biases in calculated ice-shelf mass balance, erroneous depths of the grounding line, and incorrect distances for ocean heat to reach grounding lines. For numerical flow models, errors of several km in grounding line position undermine any effort at glacier flow modeling since zero basal shear will be imposed on large sectors of grounded ice, or basal shear will be imposed on large areas that are actually afloat. A direct and accurate positioning of grounding line is critical for ice sheet studies.

[19] As mentioned earlier, a single interferogram yields errors in grounding line mapping of several km on fast-moving ice. Despite its additional data requirements, the DInSAR method is essential. The existing data have been sufficient to yield a complete mapping of grounding lines

around Antarctica and also reveal areas of large, recurrent migrations (e.g., Totten, Slessor, Bailey), with important implications for the study of their ice dynamics. We also detected the rapid grounding line retreat of several major glaciers that drive a large part of the ice sheet mass budget (e.g., Pine Island, Thwaites, Smith glaciers). These early indications of glacier instability preceded more involved measurements of lowering in surface elevation, glacier acceleration or changes in the gravity field.

5. Conclusions

[20] We present a first, complete, high-precision, uniform sampling, seamless mapping of grounding lines around Antarctica based on 15 years of DInSAR data. The results reveal major uncertainties in prior mappings that redefine the coastal outline of Antarctica's fast moving glaciers. The DInSAR map will be available at the National Snow and Ice Data Center and will be regularly updated. The usage of earlier delineations will introduce large biases in calculated ice fluxes, the set up of numerical ice flow models, the analysis of ice ocean interactions, or simply the selection of a drill site near an ice stream grounding zone. A systematic mapping and monitoring of ice sheet grounding lines with DInSAR is useful for glaciology, but also for oceanography, hydrology and geology in Antarctica. Future DInSAR missions, including ESA's Sentinel-1 in 2012 and NASA's DESDynI in 2017–2019, will provide the first continuous, frequent DInSAR coverage of grounding lines as an essential complement to the mapping of glacier velocities.

[21] **Acknowledgments.** This work was performed at the Earth System Science Department of Physical Sciences, University of California Irvine and at the California Institute of Technology's Jet Propulsion Laboratory under a contract with the National Aeronautics and Space Administration's Cryospheric Science Program and satellite data grants from ESA, JAXA, CSA, MDA and ASF.

[22] The Editor thanks Sridhar Anandakrishnan and an anonymous reviewer for their assistance in evaluating this paper.

References

- Bamber, J. L., J. L. Gomez-Dans, and J. A. Griggs (2009), A new 1 km digital elevation model of the Antarctic derived from combined satellite radar and laser data—Part 1: Data and methods, *Cryosphere*, 3(1), 101–111.
- Bohlander, J., and T. Scambos (2007), Antarctic coastlines and grounding line derived from MODIS Mosaic of Antarctica (MOA), digital media, Natl. Snow and Ice Data Cent., Boulder, Colo.
- Brunt, K., H. A. Fricker, L. Padman, T. Scambos, and S. O'Neil (2010), Mapping the grounding zone of the Ross Ice Shelf, Antarctica, using ICESat laser altimetry, *Ann. Glaciol.*, 51, 71–79.
- Budd, W. F., M. J. Corry, and T. H. Jacka (1982), Results from the Amery Ice Shelf project, *Ann. Glaciol.*, 3, 36–41.
- Frezzotti, M., A. Cimbelli, and J. G. Ferrigno (1998), Ice-front change and iceberg behaviour along Oates and George V coasts, Antarctica, 1912–96, *Ann. Glaciol.*, 27, 643–650.
- Fricker, H. A., et al. (2009), Mapping the grounding zone of the Amery Ice Shelf, East Antarctica using DInSAR, MODIS and ICESat, *Antarct. Sci.*, 21(5), 515–532.
- Gillet-Chaulet, F., and G. Durand (2010), Glaciology: Ice sheet advances in Antarctica, *Nature*, 467, 794–795.
- Goldstein, R. M., H. Engelhardt, B. Kamb, and R. Frolich (1993), Satellite radar interferometry for monitoring ice sheet motion: Application to an Antarctic ice stream, *Science*, 262, 1525–1530.
- Gray, L., et al. (2002), RADARSAT interferometry for Antarctic grounding-zone mapping, *Ann. Glaciol.*, 34, 269–276.
- Haran, T., J. Bohlander, T. Scambos, T. Painter, and M. Fahnestock (2006), MODIS mosaic of Antarctica (MOA) image map, digital media, Natl. Snow and Ice Data Cent., Boulder, Colo.

- Horgan, H. J., and S. Anandakrishnan (2006), Static grounding lines and dynamic ice streams: Evidence from the Siple Coast, West Antarctica, *Geophys. Res. Lett.*, 33, L18502, doi:10.1029/2006GL027091.
- Joughin, I., and J. L. Bamber (2005), Thickening of the ice stream catchments feeding the Filchner-Ronne Ice Shelf, Antarctica, *Geophys. Res. Lett.*, 32, L17503, doi:10.1029/2005GL023844.
- Michel, R., and E. Rignot (1999), Flow of Glaciar Moreno, Argentina, from repeat-pass Shuttle Imaging Radar images: Comparison of the phase correlation method with radar interferometry, *J. Glaciol.*, 45(149), 93–100.
- Reeh, N., E. Lintz Christensen, C. Mayer, and O. B. Olesen (2003), Tidal bending of glaciers: A linear viscoelastic approach, *Ann. Glaciol.*, 37, 83–89.
- Rignot, E. (1996), Tidal flexure, ice velocities and ablation rates of Petermann Gletscher, Greenland, *J. Glaciol.*, 42(142), 476–485.
- Rignot, E. (1998a), Fast recession of a West Antarctic glacier, *Science*, 281(5376), 549–551.
- Rignot, E. (1998b), Hinge-line migration of Petermann Gletscher, north Greenland, detected using satellite-radar interferometry, *J. Glaciol.*, 44(148), 469–476.
- Rignot, E. (2001), Evidence for rapid retreat and mass loss of Thwaites Glacier, West Antarctica, *J. Glaciol.*, 47(157), 213–222.
- Rignot, E. (2002), Mass balance of East Antarctic glaciers and ice shelves from satellite data, *Ann. Glaciol.*, 34, 217–227.
- Rignot, E., and S. Jacobs (2002), Rapid bottom melting widespread near Antarctic Ice Sheet grounding lines, *Science*, 296(5575), 2020–2023.
- Rignot, E., S. P. Gogineni, W. B. Krabill, and S. Ekholm (1997), North and northeast Greenland ice discharge from satellite radar interferometry, *Science*, 276(5314), 934–937.
- Rignot, E., et al. (2004), Improved estimation of the mass balance of glaciers draining into the Amundsen Sea sector of West Antarctica from the CECS/NASA 2002 campaign, *Ann. Glaciol.*, 39, 231–237.
- Rignot, E., et al. (2008), Recent Antarctic ice mass loss from radar interferometry and regional climate modelling, *Nat. Geosci.*, 1, 106–110.
- Schmeltz, M., E. Rignot, and D. MacAyeal (2001), Ephemeris grounding as a signal of ice-shelf change, *J. Glaciol.*, 47(156), 71–77.
- Schmeltz, M., E. Rignot, and D. MacAyeal (2002), Tidal flexure along ice-sheet margins: Comparison of DInSAR with an elastic-plate model, *Ann. Glaciol.*, 34, 202–208.
- Smith, A. M. (1991), The use of tiltmeters to study the dynamics of Antarctic ice shelf grounding lines, *J. Glaciol.*, 37(125), 51–58.
- Swithinbank, C. (1988), Satellite image atlas of glaciers of the world, *U.S. Geol. Surv. Prof. Pap.*, 1386-B, 278 pp.
- Sykes, H., T. Murray, and A. Luckman (2009), The location of the grounding zone of Evans Ice Stream, Antarctica, investigated using SAR interferometry and modelling, *Ann. Glaciol.*, 50, 35–40.
- Thomas, R. H., E. Rignot, P. Kanagaratnam, W. Krabill, and G. Casassa (2004), Force-perturbation analysis of Pine Island Glacier, Antarctica, suggests cause for recent acceleration, *Ann. Glaciol.*, 39, 133–138.
- Vaughan, D. G., A. M. Smith, P. C. Nath, and E. Le Meur (2003), Acoustic impedance and basal shear stress beneath four Antarctic ice streams, *Ann. Glaciol.*, 36, 225–232.
- Vieli, A., and A. J. Payne (2005), Assessing the ability of numerical ice sheet models to simulate grounding line migration, *J. Geophys. Res.*, 110, F01003, doi:10.1029/2004JF000202.

J. Mouginot, E. Rignot, and B. Scheuchl, Department of Earth System Science, University of California, Croul Hall, Irvine, CA 92697, USA.
(erignot@uci.edu)